

Detectability of High-Redshift Superluminous Supernovae with Upcoming Optical and Near-Infrared Surveys - II. Beyond $z=6$

Masaomi Tanaka^{1*}, Takashi J. Moriya^{2,3,4}, and Naoki Yoshida^{5,3}

¹*National Astronomical Observatory of Japan, Mitaka, Tokyo 181-8588, Japan*

²*Department of Astronomy, Graduate School of Science, University of Tokyo, 7-3-1 Hongo, Bunkyo-ku, Tokyo 113-0033, Japan*

³*Kavli Institute for the Physics and Mathematics of the Universe (WPI), Todai Institutes for Advanced Study, the University of Tokyo, Kashiwa, Chiba 277-8583, Japan*

⁴*Research Center for the Early Universe, Graduate School of Science, University of Tokyo, 7-3-1 Hongo, Bunkyo-ku, Tokyo 113-0033, Japan*

⁵*Department of Physics, Graduate School of Science, University of Tokyo, 7-3-1 Hongo, Bunkyo-ku, Tokyo 113-0033, Japan*

Accepted —. Received —

ABSTRACT

Observational identification of the first stars is one of the great challenges in the modern astronomy. Although a single first star is too faint to be detected, supernova explosions of the first stars can be bright enough. An important question is whether such supernovae can be detected in the limited observational area with realistic observational resources. We perform detailed simulations to study the detectability of superluminous supernovae (SLSNe) at high redshifts, using the observationally-calibrated star formation rate density and supernova occurrence rate. We show that a 100 deg² survey with the limiting magnitude of 26 mag in near-infrared wavelengths will be able to discover about 10 SLSNe at $z > 10$. If the survey is extended to 200 deg² with 27 mag depth, about 10 SLSNe can be discovered at $z > 15$. We emphasize that the observations at $\geq 3 \mu\text{m}$ are crucial to detect and select SLSNe at $z > 10$. Our simulations are also applied to the planned survey with Euclid, WFIRST, and WISH. These surveys will be able to detect about 1000, 400, and 3000 SLSNe up to $z \sim 5, 7, \text{ and } 12$, respectively. We conclude that detection of SLSNe at $z > 10$ is in fact achievable in the near future.

Key words: dark ages, reionization, first stars – early Universe – supernovae: general

1 INTRODUCTION

The first stars, or Population III stars, are predicted to be formed at redshift $z \gtrsim 15$ in the standard cold dark-matter scenario (e.g., Bromm, Coppi & Larson 1999; Abel, Bryan & Norman 2000; Yoshida et al. 2003; O’Shea & Norman 2007; Turk, Abel & O’Shea 2009; Stacy, Greif & Bromm 2010; Bromm et al. 2009; Bromm & Yoshida 2011; Greif et al. 2011; Clark et al. 2011). Observational identification of the first stars is one of the great challenges in the modern astronomy. In fact, a cluster of first stars can be detected in the future with the next-generation telescopes, such as James Webb Space Telescope (JWST, see e.g., Bromm, Kudritzki & Loeb 2001; Gardner et al. 2006). However, an isolated, single

first star is too faint to be observed (Gardner et al. 2006; Rydberg et al. 2013).

Detecting supernova (SN) explosions of the first stars is an interesting possibility worth pursuing. A single SN explosion can give rise to a luminosity of $L \gtrsim 10^9 L_\odot$, powered by the radioactive energy or the kinetic energy of the explosion. Note that the luminosity of SNe is comparable to high-redshift galaxies recently discovered with Hubble Space Telescope (HST, e.g., Bouwens et al. 2011a). This is more than a few orders of magnitude higher than the luminosity of a single very massive star ($L \sim 10^7 L_\odot$ for a 500 M_\odot star, Bromm, Kudritzki & Loeb 2001).

Because of this advantage, detectability of SNe at high redshift have been studied in the past literature (e.g., Miralda-Escude & Rees 1997; Mesinger, Johnson & Haiman 2006; Whalen et al. 2013c). These studies revealed, however, that normal core-collapse SNe are too faint to be detected at $z > 6$. Detection of

* E-mail: masaomi.tanaka@nao.ac.jp

normal SNe at $z > 6$ requires observations deeper than 30 AB mag in near-infrared (NIR) wavelengths, which can be reached only with a long exposure of JWST ($\sim 2 \times 10^4$ seconds for 5σ significance).

In this circumstance, several literatures (Scannapieco et al. 2005; Pan, Loeb & Kasen 2012; Pan, Kasen & Loeb 2012; Hummel et al. 2012; Whalen et al. 2012, 2013b; de Souza et al. 2013) have examined the detectability of pair-instability SNe (PISNe, see e.g., Heger & Woosley 2002; Kasen, Woosley & Heger 2011; Dessart et al. 2013). PISNe give rise to an extremely high luminosity ($L \sim 10^{10} L_{\odot}$) powered by $> 1\text{--}10 M_{\odot}$ of ^{56}Ni , and, they can be as bright as $\sim 26\text{--}27$ AB mag in NIR at $z \gtrsim 10$ (Whalen et al. 2012, 2013b). These works in part were motivated by the discovery of a PISN candidate SN 2007bi (Gal-Yam et al. 2009; Young et al. 2010). It is noted that there is ongoing debate on typical masses of Population III stars. Theoretically, both very massive stars ($\gtrsim 100 M_{\odot}$, as massive as progenitor of PISNe, e.g., Bromm, Coppi & Larson 1999; Abel, Bryan & Norman 2000) and ordinary massive stars ($\lesssim 50 M_{\odot}$, e.g., Yoshida, Omukai & Hernquist 2007; Hosokawa et al. 2011) might have existed in the early universe. Observationally, the existence of ordinary massive stars are corroborated by chemical abundances of metal poor stars (e.g., Frebel, Johnson & Bromm 2009, see Ren, Christlieb & Zhao 2012 for ongoing search of PISN signature).

The recent discovery of superluminous supernovae (SLSNe) (see Quimby et al. 2011; Gal-Yam 2012, and references therein) opens a new window to observe SN explosions of the first stars. SLSNe are thought to be powered by a huge amount of ^{56}Ni (Umeda & Nomoto 2008; Young et al. 2010; Moriya et al. 2010) and/or strong interaction with the circumstellar material (CSM). The latter is supported by characteristic Type IIn spectra, e.g., narrow hydrogen emission lines, in some SLSNe-II (SLSN with hydrogen, according to the classification by Gal-Yam 2012), such as SNe 2006gy (Ofek et al. 2007; Smith et al. 2007, 2008; Agnoletto et al. 2009; Kawabata et al. 2009) and 2008fz (Drake et al. 2010). Numerical simulations of radiation hydrodynamics of SN explosion with dense CSM have been performed by Moriya et al. (2013, hereafter M13), who found that their models can reproduce the light curve of SN 2006gy. Thanks to the high luminosity, SLSNe are ideal targets at high redshift Universe. In fact, a few SLSNe and luminous Type IIn SNe have been detected at $z \sim 2\text{--}4$ (Cooke et al. 2009, 2012).

It has been argued by Cooke (2008); Quimby et al. (2011); M13; Whalen et al. (2013a) that SLSNe and luminous Type IIn SNe are bright enough to be detected at $z > 4$. However, SLSNe are known to be extremely rare ($\sim 10^{-3}$ of core-collapse SNe, Quimby et al. 2011; Gal-Yam 2012; Quimby et al. 2013). Thus, an important question still remains; is there enough number of high-redshift SNe in the limited observational area that can be observed with realistic observational resources?

Earlier in our paper (Tanaka et al. 2012, hereafter Paper I), we studied the detectability of high-redshift SLSNe in the limited observational area for the first time. We showed about 100 SLSNe up to $z \sim 4$ can be detected with upcoming Subaru/Hyper Suprime-Cam (HSC) Deep survey, which

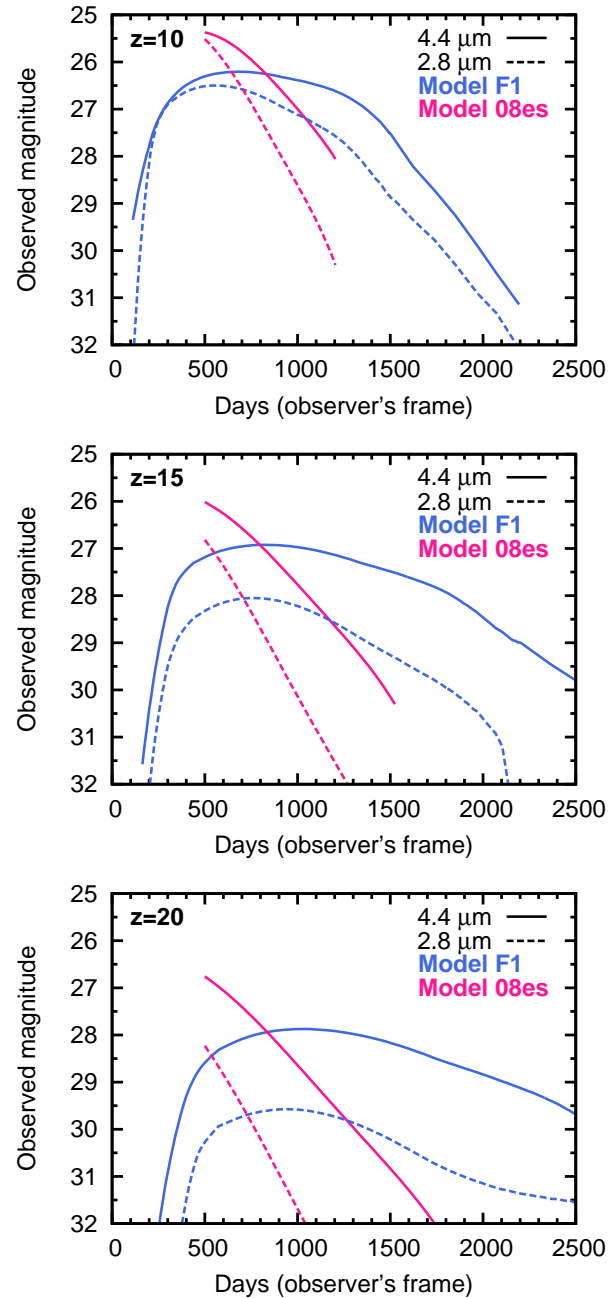


Figure 1. Observed-frame light curves of Model F1 (blue) and SN 2008es (pink) at redshift $z = 10$ (top), 15 (middle), and 20 (bottom). The solid and dashed lines represent the magnitude in $4.4 \mu\text{m}$ and $2.8 \mu\text{m}$, respectively.

reaches 24.5 mag depth in z -band. By using Ultra Deep survey for 3.5 deg^2 (25.6 mag in z -band), the maximum redshift can be as high as $z \sim 5$. We also showed that deep NIR survey can detect SLSNe even at $z \sim 6$.

In the present paper, we extend the study of Paper I to redshifts beyond $z = 6$, which is near the end of reionization of the Universe, with a special emphasis on $z > 10$, the era of the first star formation. We first describe our models for SLSNe in Section 2. The method and setup for mock observations are described in Section 3. Results of simulations are presented in Section 4. Based on the results, the optimized

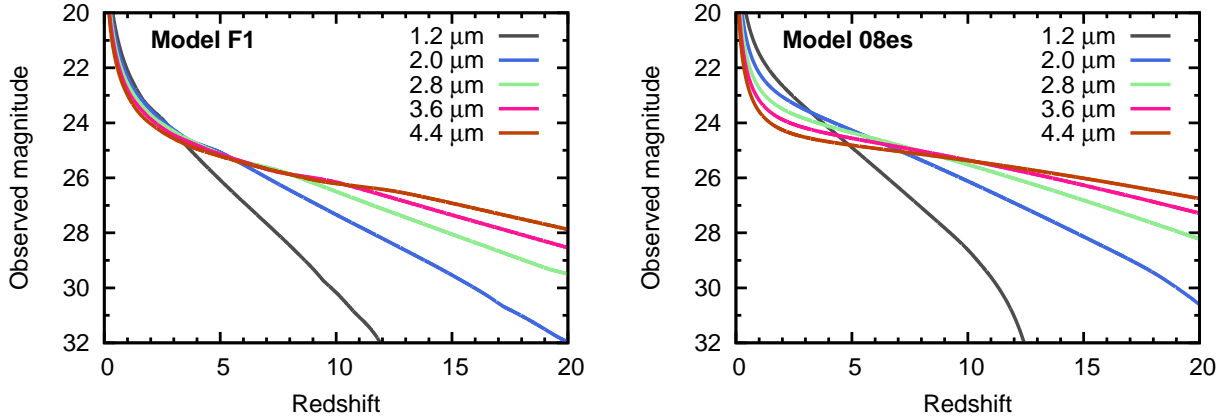


Figure 2. Observed peak magnitude of Model F1 (left) and SN 2008es (right) as a function of redshift. To detect SNe at $z > 10$, the observations at $> 3 \mu\text{m}$ are crucial. A typical limiting magnitude per visit with the planned wide-field NIR satellites is 24–26 mag (see Section 7). The faintest limit of each panel (32 mag) corresponds to $\sim 10^6$ s integration with JWST.

the survey area, and (4) the detection limit per visit. Note that the detection limit per visit does not necessarily match the limiting magnitude of each observation. The limiting magnitude can also be that of the stacked images for a period within the cadence. Considering the light curves in Figure 1, we keep 3-year survey duration and 3-month cadence unless otherwise mentioned. We explore a variety of the survey area and detection limit.

In this paper, we focus on SNe at $z > 6$. Thus, the observation in NIR wavelengths is a natural choice. We first assume simultaneous observations at 1–5 μm with 5 broadband filters in Sections 4 and 5. Then, we also perform simulations with planned sets of filters in Section 7. As shown in Figure 2, we note that observations around 1 μm are not essential to detect high-redshift SNe. For the bandpass filters, we adopt those of JWST/NIRCAM; F115W, F200W, F277W, F356W, and F444W although the observations with JWST are not necessarily assumed. For the detection limit, we assume the same limiting magnitude in these 5 filters. We do not consider the effect of host galaxy contamination to the limiting magnitudes.

We impose stringent detection criteria as in Paper I. Our definition of detection is fulfilling *both* of the following two criteria; (1) brighter than the detection limit in more than 2 bands at least at one epoch, *and* (2) brighter than the limiting magnitude at more than 3 epochs at least in one band.

3.2 Rate of Superluminous Supernovae

A key ingredient of our simulations is cosmic occurrence rate of SLSNe at high redshifts. It is reasonable to assume that the occurrence rate is proportional to the cosmic star formation rate (SFR) density ρ_* . We adopt the SFR density derived from existing observations. Figure 3 shows various measurements of SFR density using galaxies (Bouwens et al. 2011a,b; Zheng et al. 2012; Bouwens et al. 2012; Coe et al. 2013; Ellis et al. 2013) and gamma-ray bursts (GRBs, Ishida, de Souza & Ferrara 2011; Robertson & Ellis 2012). To cover the possible range of the SFR density, we adopt two cases; (A) SFR density model by Robertson & Ellis (2012),

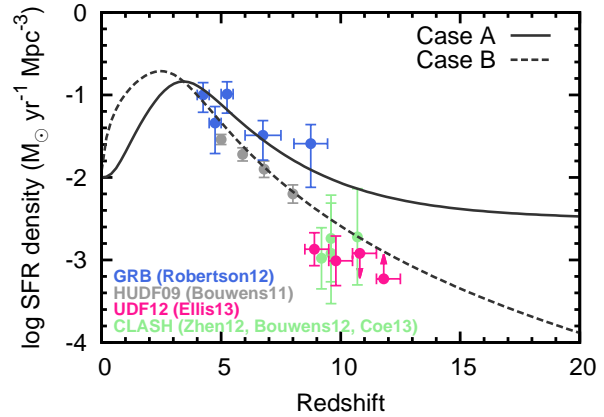


Figure 3. The SFR density estimated by galaxies (Bouwens et al. 2011a,b; Zheng et al. 2012; Bouwens et al. 2012; Coe et al. 2013; Ellis et al. 2013) and GRBs (Robertson & Ellis 2012). We test two cases of the SFR density (solid and dashed lines for Cases A and B, respectively). Case A is the SFR density model by Robertson & Ellis (2012), which is the lower bound of the SFR density derived from GRBs. Case B is a simple extrapolation of the formula by Hopkins & Beacom (2006), which is consistent with the galaxy measurements.

which is consistent with the lower bound of the SFR density derived from GRBs (solid line in Figure 3), and (B) model by Hopkins & Beacom (2006) extended to $z = 20$ (dashed line).

Since the progenitors of SLSNe are thought to be massive stars, the delay time is negligible. With this assumption, the rate of SLSNe (R_{SLSN}) can be written using ρ_* as

$$R_{\text{SLSN}}(z) = f_{\text{SLSN}} \rho_*(z) \frac{\int_{M_{\text{min,SLSN}}}^{M_{\text{max,SLSN}}} \psi(M) dM}{\int_{M_{\text{min}}}^{M_{\text{max}}} M \psi(M) dM}, \quad (1)$$

where $\psi(M)$ is the stellar initial mass function (IMF, $\psi(M) \propto M^{-(\Gamma+1)}$). We adopt a modified Salpeter A IMF of Baldry & Glazebrook (2003) with the slope $\Gamma = 0.5$ for $0.1M_{\odot} (= M_{\text{min}}) < M < 0.5M_{\odot}$ and $\Gamma = 1.35$ for $0.5M_{\odot} < M < 100M_{\odot} (= M_{\text{max}})$.

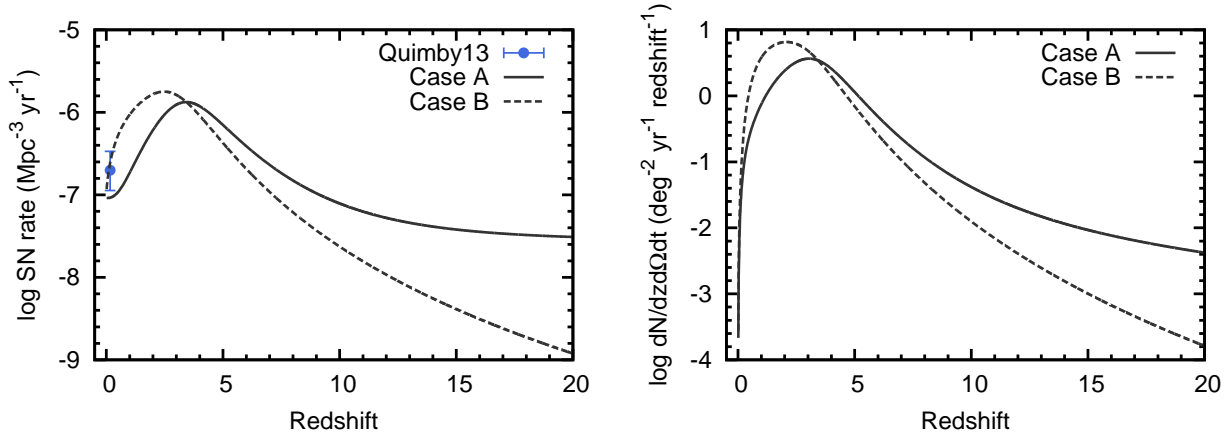


Figure 4. (Left) The cosmic occurrence rate of SLSNe per unit volume. The solid and dashed lines represent Cases A and B SFR density models. Blue point is the observed total SLSN rate by Quimby et al. (2013). (Right) SLSN rate per unit area and per unit time in the *observer's frame*.

As in Paper I, we assume that (1) from the wide mass range of stars, only massive stars with the mass of $M_{\max, \text{SLSN}} = 50M_{\odot} - M_{\max, \text{SLSN}} = 100M_{\odot}$ can be a potential progenitor of SLSNe, and (2) a fraction f_{SLSN} of such massive stars actually explode as SLSNe². The fraction f_{SLSN} can be calibrated by the observational constraints of the SLSN rate. Quimby et al. (2013) estimated the rate of SLSNe to be $2 \times 10^{-7} \text{ Mpc}^{-3} \text{ yr}^{-1}$ at $z \sim 0.2$ ³. Adopting the SFR density from Hopkins & Beacom (2006), this rate is obtained if f_{SLSN} is set to be 2×10^{-2} for $M_{\max, \text{SLSN}} = 50M_{\odot}$. This fraction corresponds to 10^{-3} of total core-collapse SNe (with the progenitor mass range of $M = 8 - 100M_{\odot}$). Hereafter we use this value of f_{SLSN} for both Cases A and B SFR density. Since redshift evolution of this fraction is poorly understood both observationally and theoretically, f_{SLSN} is assumed to be constant over redshifts. Possible impact of different IMFs is briefly discussed in Section 7 (see also Paper I). Note that Paper I adopted $f_{\text{SLSN}} = 2 \times 10^{-3} - 2 \times 10^{-2}$, which gave conservative estimates.

The left panel of Figure 4 shows the SN rate per unit comoving volume as a function of redshift. The solid and dashed lines represent the SN rate with Cases A and B SFR density, respectively. The SN rate with Case B SFR density is consistent with the observed rate of SLSNe (blue point, Quimby et al. 2013). The adopted SN rates are also roughly consistent with the rate $\sim 4 \times 10^{-7} \text{ Mpc}^{-3} \text{ yr}^{-1}$ derived using a single detection at $z \sim 2$ and 4 by Cooke et al. (2012) although this rate may not represent the total SLSN rate. The right panel of Figure 4 shows the SN rate per unit area of the sky per redshift and per unit time in the observer's frame. The expected number of SNe is an order of $0.01 \text{ deg}^{-2} \text{ yr}^{-1} \text{ redshift}^{-1}$ at $z > 10$.

² Since at least one progenitor of Type IIIn SN is known to be as massive as $M_{\text{ZAMS}} > 50 - 80M_{\odot}$ (Gal-Yam et al. 2007; Gal-Yam & Leonard 2009), we set the minimum mass of SLSNe to be $M_{\max, \text{SLSN}} = 50M_{\odot}$.

³ Although Quimby et al. (2013) derived the rates of SLSN-I (SLSN without hydrogen, $3 \times 10^{-8} \text{ Mpc}^{-3} \text{ yr}^{-1}$) and SLSN-II (SLSN with hydrogen, $1.5 \times 10^{-7} \text{ Mpc}^{-3} \text{ yr}^{-1}$) separately, we simply use the total rate.

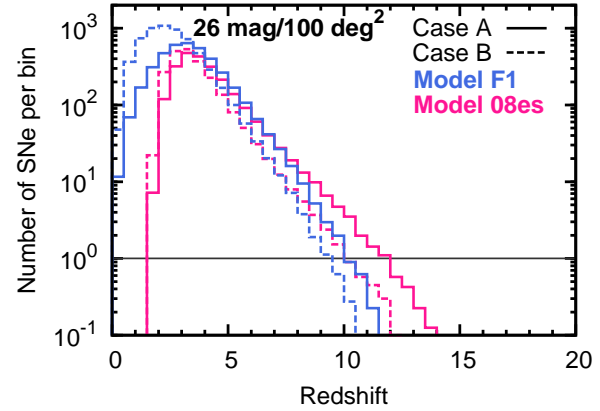


Figure 5. Expected number of SN detection per $dz = 0.5$ bin as a function of redshift with the survey area of 100 deg^2 and the limiting magnitude of 26 mag in $1-5 \mu\text{m}$. The solid and dashed lines show the dependence on the adopted SFR density (Cases A and B, respectively). The blue and red lines represent Model F1 and Model 08es, respectively.

4 RESULTS

We first show the results of our fiducial survey; observations with the survey area of 100 deg^2 , and the limiting magnitude of 26 mag. The survey duration and cadence are set to be 3 years and 3 months, respectively. Figure 5 shows the expected number of SNe per $dz = 0.5$ bin as a function of redshift. The expected number of SNe at $z > 10$ is an order of 1-10 with Model 08es (red lines in Figure 5).

The solid and dashed lines show the dependence on the adopted SFR density (Cases A and B, respectively). The expected number with the Case A SFR density is higher than that with Case B by a factor of about 3 at $z > 6$, as expected from Figures 3 and 4.

Figure 6 shows the dependence on the limiting magnitudes. The observations deeper than 27 mag at $> 3\mu\text{m}$ are deep enough not to miss SLSNe at $z \sim 15$ (see also Figure 2). With 100 deg^2 area, SLSNe beyond $z = 15$ can be detected.

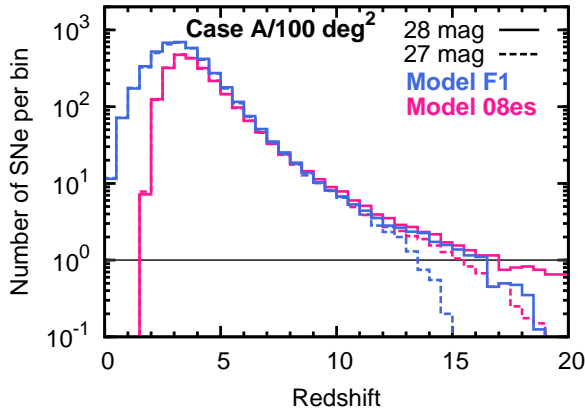


Figure 6. Expected number of SN detection per $dz = 0.5$ bin as a function of redshift with the survey area of 100 deg^2 and the limiting magnitude of 27 mag (solid line) and 28 mag (dashed line) in $1\text{-}5 \mu\text{m}$. Case A SFR density is adopted. The blue and red lines represent Model F1 and Model 08es, respectively.

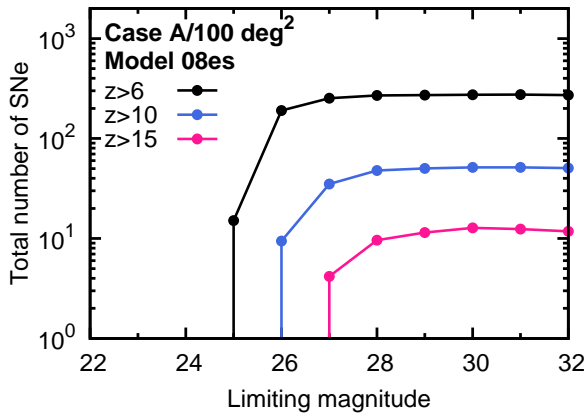


Figure 7. Expected total number of SLSNe beyond $z = 6$ (black), 10 (blue), and 15 (red) as a function of limiting magnitude. Case A SFR density and Model 08es are adopted.

Figure 7 summarizes the expected number of SLSNe beyond $z = 6$ (black), 10 (blue), and 15 (red) as a function of limiting magnitude for the case of 100 deg^2 survey area. The Case A SFR density and Model 08es are adopted. This figure leads us to conclude the following. (1) To detect SLSNe at $z > 6$, 10, and 15, observations deeper than 25, 26, and 27 mag are required, respectively. (2) Observations deeper than 28 mag are not needed to increase the number of SLSNe. Especially, the latter suggests that *in order to discover high-redshift SLSNe efficiently, observational resources should be devoted to enlarge the survey area, instead of making the observation deeper than 28 mag*. The optimized survey strategy is discussed in the next section.

5 OPTIMIZED SURVEY STRATEGY

Since observational resources are limited, it is important to find an optimized survey strategy. In general, survey observations can be characterized by (1) survey area and (2)

survey depth. For the case of transient survey, (3) cadence is another important factor. However, SLSNe at high redshifts have a long timescale (Figure 1), and thus, the requirement for the cadence is not strong (we fix the cadence to be 3 months in all the simulations presented so far). Thus, optimization of the survey strategy means finding the best combination of the survey area and depth to maximize the number of SLSNe.

Figure 8 shows the expected total number of SLSNe at $z > 6$ (upper), 10 (lower left) and 15 (lower right) in the two-dimensional plane of the survey area and depth (see Appendix for similar simulations for optical surveys). The contours show the survey area and depth giving 1, 10, and 100 SLSNe (from left bottom to right top). Figure 8 includes the survey area up to the whole sky. Note that, in actual survey, the visibility of the sky that can be visited multiple times during the survey period is limited. When observations with a NIR satellite are considered, a typical maximum area with nearly permanent visibility is about 1000 deg^2 around the ecliptic poles.

The contours are nearly vertical around 25 mag ($z > 6$), 26 mag ($z > 10$), and 27 mag ($z > 15$). This clearly indicates that, irrespective of the survey area, observations at least deeper than 25 mag, 26 mag and 27 mag are required to detect SLSNe at $z > 6$, 10, and 15, respectively (see also Figure 7). On the other hand, the contour becomes horizontal at limiting magnitudes deeper than 28 mag. This indicates that, for a given survey area, observations deeper than 28 mag do not increase the number of SNe.

The gray dashed lines in Figure 8 represent the combination of the survey area and depth for a given survey power (i.e., $A\Omega t$, a product of certain set of photon-correction power A , field of view Ω , and observational time t). From the comparison with simulations, we conclude that the optimized survey strategy to detect more than 10 SLSNe at $z > 10$ would be *100 deg² survey with the limiting magnitude of 26 mag*.

In order to detect more than 10 SLSNe at $z > 15$, wider and deeper survey should be performed. The optimized strategy would be *200 deg² survey with the limiting magnitude of 27 mag*. Compared with the survey to detect 10 SLSNe at $z > 10$, the survey power $A\Omega t$ should be increased by a factor of ~ 13 .

Our results can also be applied for PISNe. The existence or occurrence rate of PISNe are not established well, and the predicted rates have a wide range: $10^{-2} - 1 \text{ deg}^{-2} \text{ yr}^{-1} \text{ redshift}^{-1}$ (Wise & Abel 2005; Weinmann & Lilly 2005; Johnson, Dalla & Khochfar 2013). Note that these rates may increase by the effect of rotation of progenitor stars (Chatzopoulos & Wheeler 2012). When the prediction by Johnson, Dalla & Khochfar (2013) is adopted, the rate is $10^{-2} - 10^{-1} \text{ deg}^{-2} \text{ yr}^{-1} \text{ redshift}^{-1}$, which is similar to the expected SLSN rate (Figure 4). According to the calculations by Whalen et al. (2012, 2013b), the peak brightness of some PISN models is as bright as 26 mag at $z = 10$ and 27 mag at $z = 15$ in the NIR wavelengths, which are also similar to those of SLSNe (Figures 1 and 2). In this case, the same observing strategy with SLSNe will be able to discover a similar number of PISNe: a 100 deg^2 survey with the limiting magnitude of 26 mag will discover about 10 PISNe at $z > 10$, and a 200 deg^2 survey with the lim-

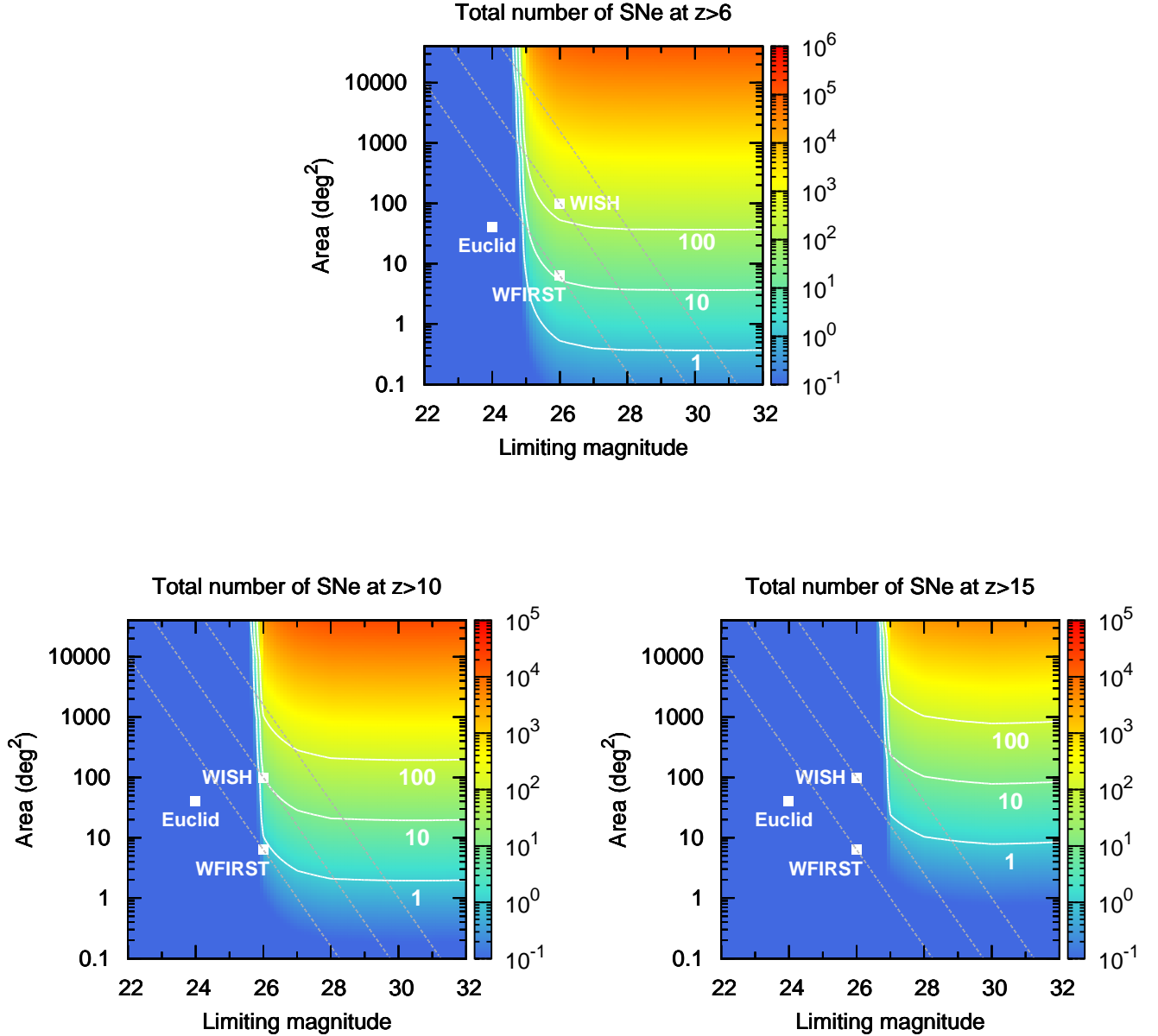


Figure 8. Expected total number of SLSNe at $z > 6$ (upper), 10 (lower left) and 15 (lower right) as a function of survey area and limiting magnitude. The contours show the combination of the survey area and limiting magnitude giving 1, 10, and 100 SLSNe (from left bottom to right top). White squares show the survey area and limiting magnitude for planned surveys (Table 1). The contours are nearly vertical at the limiting magnitudes of 25 mag ($z > 6$), 26 mag ($z > 10$), and 27 mag ($z > 15$). This indicates that the observations deeper than at least 25, 26 and 27 mag are required to detect SLSNe at $z > 6$, 10 and 15, respectively. On the other hand, the contours are horizontal at the limiting magnitude deeper than 28 mag. This indicates that, for a given survey area, observations deeper than 28 mag do not increase the number of SLSNe dramatically. The gray dashed lines represent the combination of the survey area and depth for a given survey power (i.e., Ωt). Case A SFR density and Model 08es are adopted.

iting magnitude of 27 mag will discover about 10 PISNe at $z > 15$.

6 SELECTION OF HIGH-REDSHIFT SLSNE

We discuss selection methods for SLSNe at high redshifts. Since SLSNe are rare objects, it is naturally expected that more Type Ia SNe and normal core-collapse SNe at lower redshifts will be discovered with the NIR surveys presented

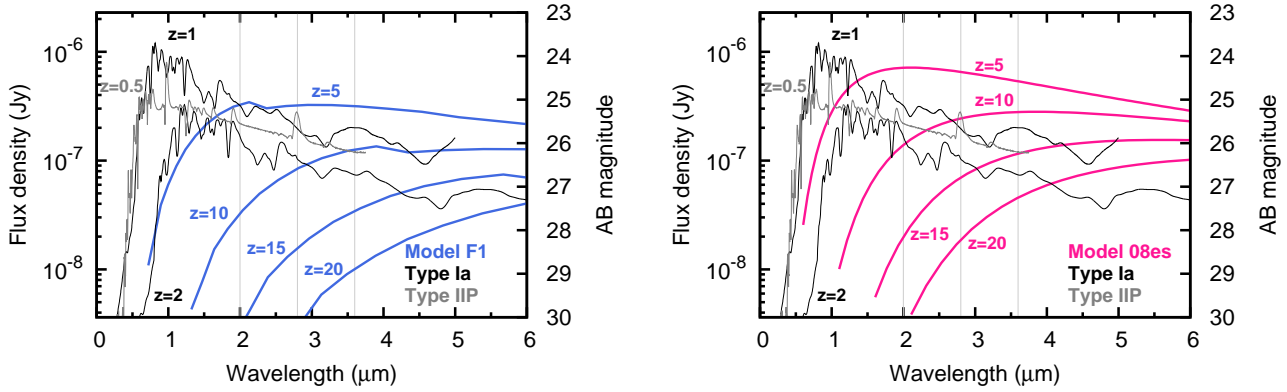


Figure 9. SEDs of Model F1 (left) and Model 08es (right) for different redshifts. For comparison, spectral templates of Type Ia SNe (black) and Type IIP SNe (gray) are also shown.

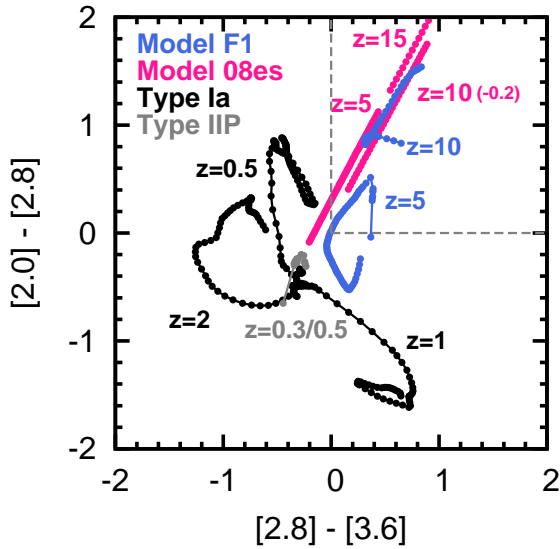


Figure 10. Color-color diagram for two SLSN models (blue and pink). They are compared with Type Ia SNe and Type IIP SNe at lower redshifts with similar observed magnitudes. SLSNe at high redshifts have a red color both in $[2.0] - [2.8]$ and $[2.8] - [3.6]$ compared with Type Ia and IIP SNe with similar observed magnitudes. Colors of Model 08es at $z = 10$ are shifted by -0.2 mag in $[2.0] - [2.8]$ color just for visibility.

in the previous sections. Thus, we must efficiently pick up candidates of high-redshift SLSNe.

A clear difference is its timescale of the variability. Because of the intrinsically long timescale and time dilation by high redshifts, the expected timescale of the variation of SLSNe is longer than 100 days (Figure 1). This is much longer than that of Type Ia SNe at lower redshifts ($z \lesssim 2$).

However, Type IIP SNe may have a similar timescale at the plateau phase. For the further selection, observations more than 2 bands are helpful. Figure 9 shows the spectral energy distribution (SED) of high-redshift SLSNe, compared with those of low-redshift Type Ia SNe (black) and Type IIP SNe (gray) with similar observed magnitudes. For the SEDs of Type Ia and IIP SNe, we use spectral tem-

plates by Nugent, Kim & Perlmutter (2002)⁴. In the NIR wavelengths, SLSNe at high redshifts are observed around the peak of the SED or at the bluer side of the peak. In contrast, Type Ia and IIP SNe are always observed at the redder side of the peak. As a result, SLSNe at high redshifts are redder than Type Ia and IIP SNe with similar observed magnitudes.

The red color of high-redshift SLSNe is more clearly seen in a color-color diagram (Figure 10). In this figure, we use bandpass filter of JWST ($[2.0]$, $[2.8]$, and $[3.6]$ are magnitudes in F200W, F277W, and F356W filters, respectively). SLSNe at high redshifts tend to have a redder color in $[2.0] - [2.8]$ and $[2.8] - [3.6]$, compared with Type Ia and IIP SNe with similar observed magnitudes. We note, however, that only with 2-band observations, confusion with Type Ia SNe are not fully solved. We emphasize that observations at $\geq 3 \mu\text{m}$ is useful not only for detection at higher redshifts, but also for the target selection. Objects having both $[2.0] - [2.8] > 0$ and $[2.8] - [3.6] > 0$ colors (dashed lines in Figure 10) are likely to be high-redshift SLSNe.

7 APPLICATION TO FUTURE SURVEYS

Based on the results shown in the previous sections, we apply our simulations to several planned surveys in the near future. We consider NIR survey with Euclid⁵, the Wide-Field Infrared Survey Telescope (WFIRST)⁶, and Wide-field Imaging Surveyor for High-redshift (WISH)⁷. Adopted survey parameters are summarized in Table 1.

Euclid plans to perform a wide ($15000\text{-}20000 \text{ deg}^2$) and deep (40 deg^2) survey (Laureijs et al. 2011). A part of deep survey may have multiple visits for Type Ia SNe, although the exact cadence is not yet fixed. The wavelength coverage is up to $2 \mu\text{m}$ (H band). The survey depth per visit is 24.5 mag in the visual band and 24.0 mag in the NIR bands. We hypothetically assume 10-day cadence and 3-year survey period. We perform mock observations with these parameters.

⁴ http://supernova.lbl.gov/~nugent/nugent_templates.html

⁵ <http://sci.esa.int/euclid>

⁶ <http://wfirst.gsfc.nasa.gov>

⁷ <http://www.wishmission.org/en/index.html>

Table 1. Parameters for upcoming NIR surveys

Survey	Area (deg ²)	Depth (mag)	Wavelength range	Cadence	Duration
Optimal ($z > 10$)	100	26.0	3-5 μ m	3 months	3 years
Optimal ($z > 15$)	200	26.0	3-5 μ m	3 months	3 years
Euclid	40	24.5 (visual), 24.0(Y, J, K)	0.55 - 2 μ m (visual - H)	10 days	3 years
WFIRST	6.5	26.0	0.73 - 2.4 μ m (Z - K)	5 days	1.8 years
WFIRST-extended	100	26.0	0.73 - 2.4 μ m (Z - K)	5 days	1.8 years
WFIRST-extended +3 μ m	100	26.0	0.73 - 3.0 μ m	5 days	1.8 years
WISH	100	26.0	1.0 - 4.5 μ m	10 days	1 year

* Limiting magnitude per visit, but it can also be the limiting magnitude in the stacked image for a given period within the cadence.

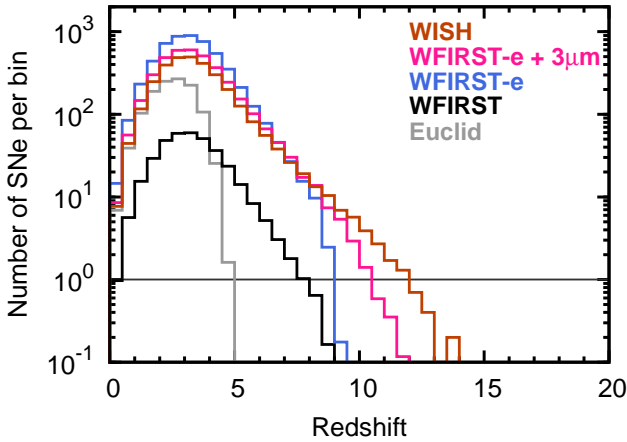


Figure 11. Expected number of SN detection per $dz = 0.5$ bin as a function of redshift with upcoming NIR surveys. For the adopted survey parameters, see Table 1. WFIRST (black and blue lines) covers the wavelength range up to K -band (2.4 μ m). If a 3 μ m-band is hypothetically added, the highest redshift will exceed $z = 10$ (pink line). Since WISH plans to cover up to 4 μ m, SNe at higher redshifts can be detected. All the simulations have been performed for Case A SFR density and Model 08es.

Throughout this section, we adopt Case A SFR density and Model 08es. The result is shown in the gray line in Figure 11. Euclid will be able to discover ~ 1000 SLSNe at $z < 5$. The maximum reachable redshift is about $z = 5$, which is limited by the 24.0 mag depth at 2 μ m (see Figure 2).

Euclid will provide an unprecedented sample of SLSNe. Since about half of SLSNe detected by Euclid are located at $z < 2$, they can also be observed with optical spectroscopy (Cooke et al. 2009, 2012). With this sample, we can study statistical properties of each class of SLSNe (SLSN-I and SLSN-II, see Quimby et al. 2011; Gal-Yam 2012), such as the luminosity function and statistics of the light curve duration, which can be used to unveil the nature and progenitors of SLSNe.

Next, we consider surveys with WFIRST. WFIRST plans to perform dedicated SN survey in a part of the observational time (Green et al. 2012). The planned survey area is 6.5 deg² (wide) and 1.8 deg² (deep). Since a large survey area is critical for the detection of SLSNe (Figure 8), we adopt 6.5 deg². The wavelength coverage is up to 2.4

μ m (K -band) and the survey depth per visit is 26.0 mag. Cadence and survey period are 5 days and 1.8 years, respectively, which are optimized for Type Ia SNe. The result of mock observation with these parameters (WFIRST, Table 1) is shown in black line in Figure 11. Thanks to the deep observations at 2.4 μ m, WFIRST will be able to discover ~ 400 SLSNe up to $z \sim 7$.

It is also shown, however, that the survey area of 6.5 deg² is not enough to fully utilize its observational depth. To see this effect, we hypothetically perform the simulations with the survey area of 100 deg² with all the other parameters kept the same (WFIRST-extended, Table 1). Such a survey dramatically increases the number of SLSNe (see Figure 8): ~ 6000 SLSNe up to $z \sim 9$ will be detected (blue line in Figure 11).

Even with the extended survey area, there is a clear cutoff in the expected number of SLSNe below $z \sim 10$. This is because the expected brightness of SLSNe in the K -band (1.8-2.4 μ m) becomes dramatically fainter at the redshifts higher than $z \sim 5$ (Figure 2). To see the advantage to have 3 μ m band, we perform a simulation by hypothetically adding 3 μ m band to the WFIRST-extended survey (pink line in Figure 11). If WFIRST possibly covers 3 μ m, it will be able to carry out the nearly ideal survey, detecting SLSNe at $z > 10$. We emphasize the importance of observations at ≥ 3 μ m.

WISH plans to focus on the deep survey with ~ 100 deg² (Yamada et al. 2012). The wavelength range is 1.0-4.5 μ m and the survey depth per visit is about 26.0 mag. Cadence and survey period are not yet fixed, and thus, we hypothetically assume 10-day cadence and 1-year survey period (see WISH in Table 1). The brown line in Figure 11 shows the expected number of SLSNe with WISH survey. WISH will be able to detect about 3000 SLSNe in total. Thanks to the wavelength coverage up to 4.5 μ m, the maximum redshift is higher than those of Euclid and WFIRST. It may be able to discover SLSNe up to $z \sim 12$. This is, in fact, quite similar to the optimized survey strategy to detect SLSNe at $z > 10$ suggested in Section 5.

WISH and extended WFIRST surveys will be able to detect more than 100 SLSNe at $z > 6$ (see also Figure 8). Such high-redshift SLSNe can be spectroscopically observed with JWST and also ground-based 30m-class telescopes, such as Thirty Meter Telescope (TMT, see e.g., Wright et al.

2010 for the expected sensitivity)⁸, Giant Magellan Telescope (GMT)⁹, and European Extremely Large Telescope (E-ELT)¹⁰. As demonstrated in Paper I, this number is sensitive to the slope of IMF (see also Cooke et al. 2009). If the slope Γ changes from 1.35 to 1.1, the expected number increases by a factor of 3. Comparison between the redshift evolution of the SLSN rate and SFR density will provide a unique method to probe top-heavy IMF at high-redshift Universe.

The planned and model surveys discussed above are not necessarily tuned to the detection of high-redshift SLSNe. Especially, the cadence is higher than that required to detect high-redshift SLSNe (see Figure 1). By stacking 3-month data of WISH or WFIRST-extended survey, the observational depth can be 27 mag in NIR. This is in fact very close to the ideal survey strategy to detect SLSNe at $z \sim 15$ (Section 5). It is emphasized that the proposed optimized survey strategy to detect SLSNe at $z > 10$ -15 can be realized with a slight modification of the planned surveys.

8 CONCLUSIONS

SN explosions of first stars are unique possibility to observationally study a single first star. We study the detectability of SLSNe at high redshifts, including the era of the first star formation. It has been suggested that SLSNe can be bright enough even at such high redshifts, but it was not clear if SLSNe can be detected for a limited observational area and with realistic observing resources.

We perform simulations of mock observations for SLSNe using the observationally-calibrated SFR densities and supernova rates. We find that a 100 deg² survey with the limiting magnitude of 26 mag will be able to discover ~ 10 SLSNe at $z > 10$. To extend the detection to $z > 15$, the survey should be extended to 200 deg² with 27 mag depth. We emphasize that the observations at $\geq 3 \mu\text{m}$ are important to detect SLSNe at $z > 10$. The observations deeper than 28 mag do not increase the number of SNe, and observational resources should be devoted to enlarge the survey area.

High-redshift SLSNe can be distinguished from lower-redshift Type Ia SNe and normal core-collapse SNe by the long timescale of variability. In addition, the red observed colors are important characteristics to select SLSNe at high redshifts. Objects that are red both in [2.0]–[2.8] and [2.8]–[3.6] color are likely to be high-redshift SLSNe. The observations at $\geq 3 \mu\text{m}$ are also important for the target selection.

We also applied our simulations to planned surveys with the wide-field NIR satellites. We find that the survey by Euclid, WFIRST, and WISH will be able to detect about 1000, 400, and 3000 SLSNe up to $z \sim 5, 7, \text{ and } 12$, respectively. It is demonstrated again that the observations at $\geq 3 \mu\text{m}$ is crucial to detect SLSNe at $z > 10$. Among these survey satellites, the observations with WISH seems the most suitable to detect high-redshift SLSNe. By stacking 3-month data, SLSNe even at $z \sim 15$ can be discovered.

⁸ <http://www.tmt.org>

⁹ <http://www.gmto.org>

¹⁰ <http://www.eso.org/public/teles-instr/e-elt.html>

We emphasize that the proposed optimized survey strategy to detect SLSNe at $z > 10$ is not far from reality. In fact, we show that the planned NIR surveys partly achieve the required specification, and that a slight modification of the planned surveys makes the surveys closer to the ideal survey to detect SLSNe at $z > 10$. We will be able to reach a single star at $z > 10$, possibly out of the first stars, with such NIR surveys in the near future. Such surveys will provide a unique way to unveil the properties of the first stars and IMF in the early Universe.

MT thanks Kohji Tsumura for useful comments. The authors are supported by the Japan Society for the Promotion of Science (JSPS) Grant-in-Aid for Young Scientists (24740117: MT, 20674003: NY), Grant-in-Aid for Scientific Research (25287050: NY), and Grant-in-Aid for JSPS Fellows (23.5929: TM). This research has been supported in part by World Premier International Research Center Initiative, MEXT, Japan.

REFERENCES

- Abel T., Bryan G. L., Norman M. L., 2000, *ApJ*, 540, 39
 Agnoletto I. et al., 2009, *ApJ*, 691, 1348
 Baldry I. K., Glazebrook K., 2003, *ApJ*, 593, 258
 Bouwens R. et al., 2012, arXiv:1211.2230
 Bouwens R. J. et al., 2011a, *Nature*, 469, 504
 —, 2011b, *ApJ*, 737, 90
 Bromm V., Coppi P. S., Larson R. B., 1999, *ApJ*, 527, L5
 Bromm V., Kudritzki R. P., Loeb A., 2001, *ApJ*, 552, 464
 Bromm V., Yoshida N., 2011, *ARA&A*, 49, 373
 Bromm V., Yoshida N., Hernquist L., McKee C. F., 2009, *Nature*, 459, 49
 Chatzopoulos E., Wheeler J. C., 2012, *ApJ*, 748, 42
 Chomiuk L. et al., 2011, *ApJ*, 743, 114
 Clark P. C., Glover S. C. O., Smith R. J., Greif T. H., Klessen R. S., Bromm V., 2011, *Science*, 331, 1040
 Coe D. et al., 2013, *ApJ*, 762, 32
 Cooke J., 2008, *ApJ*, 677, 137
 Cooke J., Sullivan M., Barton E. J., Bullock J. S., Carlberg R. G., Gal-Yam A., Tollerud E., 2009, *Nature*, 460, 237
 Cooke J. et al., 2012, *Nature*, 491, 228
 de Souza R. S., Ishida E. E. O., Johnson J. L., Whalen D. J., Mesinger A., 2013, arXiv:1306.4984
 Dessart L., Waldman R., Livne E., Hillier D. J., Blondin S., 2013, *MNRAS*, 428, 3227
 Drake A. J. et al., 2010, *ApJ*, 718, L127
 Ellis R. S. et al., 2013, *ApJ*, 763, L7
 Frebel A., Johnson J. L., Bromm V., 2009, *MNRAS*, 392, L50
 Gal-Yam A., 2012, *Science*, 337, 927
 Gal-Yam A., Leonard D. C., 2009, *Nature*, 458, 865
 Gal-Yam A. et al., 2007, *ApJ*, 656, 372
 —, 2009, *Nature*, 462, 624
 Gardner J. P. et al., 2006, *Space Sci. Rev.*, 123, 485
 Gezari S. et al., 2009, *ApJ*, 690, 1313
 Green J. et al., 2012, arXiv:1208.4012
 Greif T. H., White S. D. M., Klessen R. S., Springel V., 2011, *ApJ*, 736, 147
 Heger A., Woosley S. E., 2002, *ApJ*, 567, 532

Hogg D. W., Baldry I. K., Blanton M. R., Eisenstein D. J., 2002, arXiv:astro-ph/0210394

Hopkins A. M., Beacom J. F., 2006, ApJ, 651, 142

Hosokawa T., Omukai K., Yoshida N., Yorke H. W., 2011, Science, 334, 1250

Hummel J. A., Pawlik A. H., Milosavljević M., Bromm V., 2012, ApJ, 755, 72

Ishida E. E. O., de Souza R. S., Ferrara A., 2011, MNRAS, 418, 500

Ivezic Z. et al., 2008, arXiv:0805.2366

Johnson J. L., Dalla V. C., Khochfar S., 2013, MNRAS, 428, 1857

Kasen D., Bildsten L., 2010, ApJ, 717, 245

Kasen D., Woosley S. E., Heger A., 2011, ApJ, 734, 102

Kawabata K. S., Tanaka M., Maeda K., Hattori T., Nomoto K., Tominaga N., Yamanaka M., 2009, ApJ, 697, 747

Laureijs R. et al., 2011, arXiv:1110.3193

LSST Science Collaborations et al., 2009, arXiv:0912.0201

Mesinger A., Johnson B. D., Haiman Z., 2006, ApJ, 637, 80

Miller A. A. et al., 2009, ApJ, 690, 1303

Miralda-Escude J., Rees M. J., 1997, ApJ, 478, L57+

Miyazaki S. et al., 2006, in Society of Photo-Optical Instrumentation Engineers (SPIE) Conference Series, Vol. 6269, Society of Photo-Optical Instrumentation Engineers (SPIE) Conference Series

Moriya T., Tominaga N., Tanaka M., Maeda K., Nomoto K., 2010, ApJ, 717, L83

Moriya T. J., Blinnikov S. I., Tominaga N., Yoshida N., Tanaka M., Maeda K., Nomoto K., 2013, MNRAS, 428, 1020

Moriya T. J., Tominaga N., 2012, ApJ, 747, 118

Neill J. D. et al., 2011, ApJ, 727, 15

Nugent P., Kim A., Perlmutter S., 2002, PASP, 114, 803

Ofek E. O. et al., 2007, ApJ, 659, L13

Oguri M., Marshall P. J., 2010, MNRAS, 405, 2579

O'Shea B. W., Norman M. L., 2007, ApJ, 654, 66

Pan T., Kasen D., Loeb A., 2012, MNRAS, 422, 2701

Pan T., Loeb A., Kasen D., 2012, MNRAS, 423, 2203

Quimby R. M., Aldering G., Wheeler J. C., Höflich P., Akerlof C. W., Rykoff E. S., 2007, ApJ, 668, L99

Quimby R. M. et al., 2011, Nature, 474, 487

Quimby R. M., Yuan F., Akerlof C., Wheeler J. C., 2013, MNRAS

Ren J., Christlieb N., Zhao G., 2012, Research in Astronomy and Astrophysics, 12, 1637

Robertson B. E., Ellis R. S., 2012, ApJ, 744, 95

Rydberg C.-E., Zackrisson E., Lundqvist P., Scott P., 2013, MNRAS, 429, 3658

Scannapieco E., Madau P., Woosley S., Heger A., Ferrara A., 2005, ApJ, 633, 1031

Smith N. et al., 2008, ApJ, 686, 485

—, 2007, ApJ, 666, 1116

Stacy A., Greif T. H., Bromm V., 2010, MNRAS, 403, 45

Takahashi R., Oguri M., Sato M., Hamana T., 2011, ApJ, 742, 15

Tanaka M., Moriya T. J., Yoshida N., Nomoto K., 2012, MNRAS, 422, 2675

Turk M. J., Abel T., O'Shea B., 2009, Science, 325, 601

Umeda H., Nomoto K., 2008, ApJ, 673, 1014

Weinmann S. M., Lilly S. J., 2005, ApJ, 624, 526

Whalen D. J. et al., 2012, arXiv:1211.4979

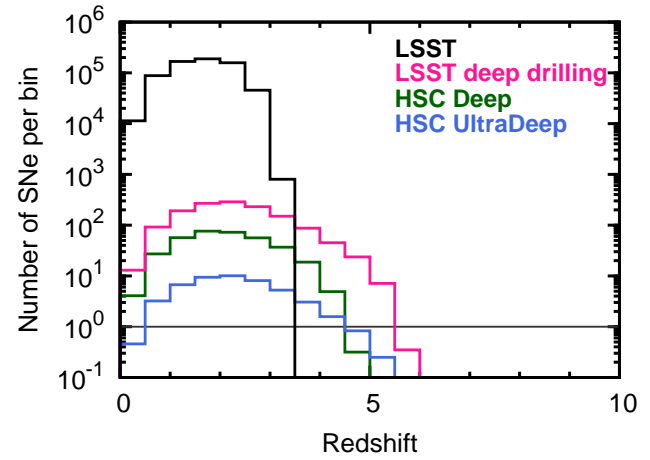


Figure A2. Expected number of SN detection per $dz = 0.5$ bin as a function of redshift with LSST surveys. For the adopted survey parameters, see Table A1. For comparison, we show the simulations with the HSC survey strategy (Deep and UltraDeep layers). In this figure, a constant limiting magnitude in optical wavelengths is assume for simplicity. See Paper I for more detailed simulations with HSC. All the simulations have been performed for Case B SFR density and Model 08es.

—, 2013a, ApJ, 768, 195

Whalen D. J., Fryer C. L., Holz D. E., Heger A., Woosley S. E., Stiavelli M., Even W., Frey L. H., 2013b, ApJ, 762, L6

Whalen D. J., Joggerst C. C., Fryer C. L., Stiavelli M., Heger A., Holz D. E., 2013c, ApJ, 768, 95

Wise J. H., Abel T., 2005, ApJ, 629, 615

Wright S. A., Barton E. J., Larkin J. E., Moore A. M., Crampton D., Simard L., 2010, in Society of Photo-Optical Instrumentation Engineers (SPIE) Conference Series, Vol. 7735, Society of Photo-Optical Instrumentation Engineers (SPIE) Conference Series

Yamada T. et al., 2012, in Society of Photo-Optical Instrumentation Engineers (SPIE) Conference Series, Vol. 8442, Society of Photo-Optical Instrumentation Engineers (SPIE) Conference Series

Yoshida N., Abel T., Hernquist L., Sugiyama N., 2003, ApJ, 592, 645

Yoshida N., Omukai K., Hernquist L., 2007, ApJ, 667, L117

Young D. R. et al., 2010, A&A, 512, A70+

Zheng W. et al., 2012, Nature, 489, 406

APPENDIX A: APPLICATION TO UPCOMING OPTICAL SURVEYS

We also apply our simulations to upcoming optical surveys. Paper I performed detailed simulations with realistic, planned observational strategy for Subaru Hyper Suprime-Cam (HSC, Miyazaki et al. 2006) survey. On the other hand, as shown in Section 5, it is useful to study a wide range of parameters to find the optimized survey strategy. In this section, we present simpler simulations for optical surveys, but with a wider parameter space.

With optical surveys, detection of SLSNe up to $z \sim 5$ is

Table A1. Parameters for upcoming optical surveys

Survey	Area (deg ²)	Depth (mag)	Cadence	Duration
HSC Deep *	30	25.0	10 days	0.5 years
HSC UltraDeep *	3.5	26.0	10 days	0.5 years
LSST	20000	**	10 days	0.25 years × 10
LSST deep drilling	100	26.0	10 days	0.5 years

* For simplicity, a constant limiting magnitude is assumed. See Paper I for more realistic simulations.

** Limiting magnitude per single visit for LSST: 23.9 (*u*), 25.0 (*g*), 24.7 (*r*), 24.0 (*i*), 23.3 (*z*), and 22.1 (*y*).

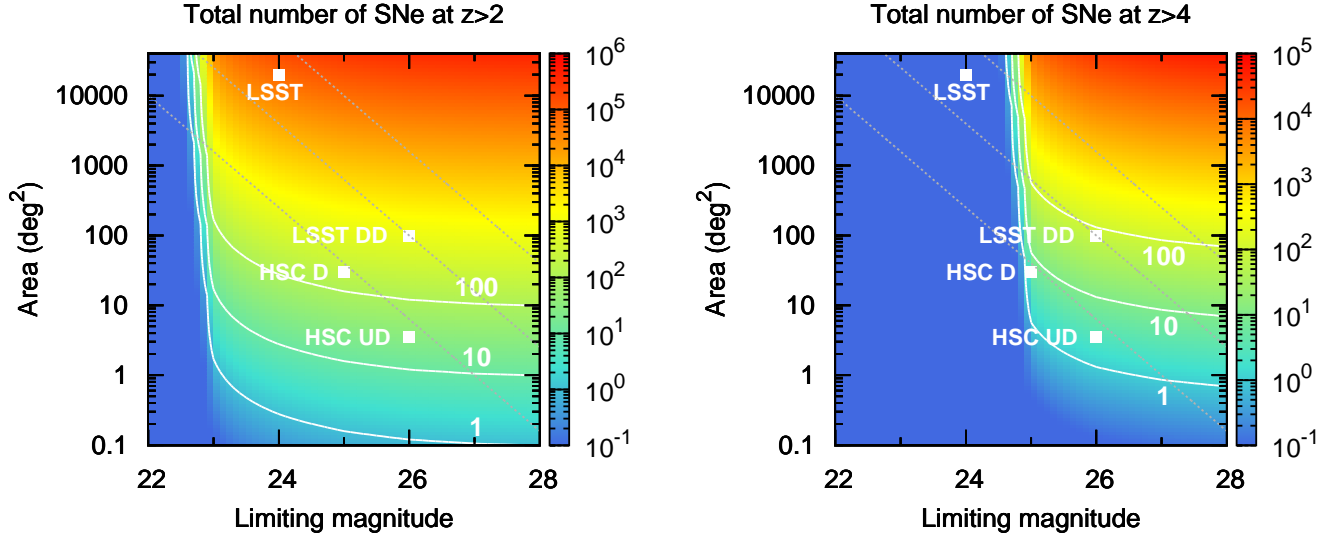


Figure A1. The same as Figure 8 but for optical surveys with 10-day cadence for 0.5 years. The left and right panels show the expected total number of SLSNe at $z > 2$ and 4, respectively. White squares show the survey area and limiting magnitude for planned optical surveys (Table A1). Case B SFR density and Model 08es are adopted.

expected (Paper I). Thus, it is natural to adopt a shorter duration of the survey and a higher cadence than those of NIR surveys. Here we simply adopt (1) 0.5-year survey and (2) 10-day cadence. For simplicity, simultaneous observations in the optical *ugrizy* bands with the same limiting magnitudes are assumed. Figure A1 shows the expected total number of SLSNe at $z > 2$ (left) and 4 (right) as a function of survey area and limiting magnitude per visit. All the simulations have been performed for Case B SFR density (better calibrated at $z < 6$ than Case A SFR density) and Model 08es.

Our simulations are also applied for planned survey with Large Synoptic Survey Telescope (LSST, Ivezić et al. 2008; LSST Science Collaborations et al. 2009). LSST will perform 20000 deg² survey in the optical *ugrizy* bands. Each visit consists of a short exposure (15 seconds), giving following limiting magnitudes; 23.9 (*u*), 25.0 (*g*), 24.7 (*r*), 24.0 (*i*), 23.3 (*z*), and 22.1 (*y*). Each patch of the sky is visited about 100-200 times for 10 years. Thus, the parameters of the survey using the single visit can be roughly approximated as (1) 3-month survey for each year (repeating for 10 years) and (2) 10-day cadence (see Table A1). The black

line in Figure A2 shows the expected number of SLSNe using the single visits of LSST. LSST will be able to discover about 10^6 of SLSNe up to $z \sim 3 - 4$. In this overwhelming sample, some SLSNe ($\gtrsim 10 - 100$) may be discovered as extremely luminous sources because of the magnification by gravitational lensing (Oguri & Marshall 2010, see also Takahashi et al. 2011).

By appropriately stacking the data, giving a deeper limiting magnitude, the maximum redshift will be higher. One promising strategy is using "deep drilling" fields of LSST. About 10 % of the observing time will be devoted to observe several deep fields. Even with 10 % of the observing time, if we limit the survey area to 100 deg² and the survey duration to 0.5 year, deep observations (with about 100 images stacked) can be performed with 10-day cadence. Such a deep image will give limiting magnitudes of about 26 mag (Table A1, LSST deep drilling). Simulations with these parameters show that LSST deep drilling observations will be able to detect about 10^3 SLSNe up to $z \sim 5 - 6$ (pink line in Figure A2).